Title

Interregional Correlations in Parkinson Disease and Parkinson-related Dementia with Resting Functional MR Imaging

Journal

Radiology, 263(1)

ISSN

0033-8419

Authors

Seibert, Tyler M

Murphy, Elizabeth A

Kaestner, Erik J

et al.

Publication Date

2012-04-01

DOI

10.1148/radiol.12111280

Peer reviewed

Radiology

Interregional Correlations in Parkinson Disease and Parkinson-related Dementia with Resting Functional MR Imaging[1]

Tyler M. Seibert, PhD
Elizabeth A. Murphy, BA
Erik J. Kaestner, BA
James B. Brewer, MD, PhD

Purpose: To apply a recently developed native-space (or native-surface) method to compare resting functional magnetic resonance (MR) imaging correlations (functional connectivity) measured in patients with Parkinson-related dementia (PRD) to those measured in cognitively unimpaired, age-matched control subjects with or without Parkinson disease (PD).

Materials and Methods: The study was approved by the institutional review board and complied with HIPAA regulations. Participants included cognitively unimpaired elderly individuals (n = 19), cognitively unimpaired patients with PD (n = 19), and patients with PRD (n = 18). Resting functional MR data were assessed by calculating correlation coefficients between blood oxygen level–dependent time series of a seed region and of other regions of interest selected a priori. Two seeds were used: a medial parietal region that contributes to the default network affected in Alzheimer disease and the caudate, which is affected by loss of dopaminergic inputs in PD. Correlation analyses were performed in the native space of individual subjects to avoid confounds from transformation to an average brain. Two-sample t tests were applied to data from each native-surface region of interest, and vertex-wise comparisons were made by using two-sample t tests at each vertex on the group surface; statistical results were corrected for multiple comparisons. Cortical thickness and striatal volumes were also compared across groups for the regions of interest.

Results: Corticostriatal functional correlations were decreased in PRD patients relative to elderly control subjects in bilateral prefrontal regions; largest difference was observed in the right caudal middle frontal region (r = 0.48 in PRD patients and 0.81 in elderly control subjects, uncorrected P = .001). Conversely, there was no significant difference across groups in the strength of default-network correlations. There was also no significant difference across groups in cortical thickness or striatal volume.

Conclusion: PRD was associated with selective disruption of corticostriatal resting functional MR imaging correlations, which suggests that resting functional MR imaging analyzed in subject-native space may be a useful biomarker in this disease. Additionally, at least in the present cohort, this technique was more sensitive to PRD changes than was quantitative structural MR imaging.

[1] From the Departments of Bioengineering (T.M.S.), Radiology (T.M.S., E.A.M., E.J.K., J.B.B.), and Neurosciences (E.A.M., J.B.B.), University of California, San Diego, 9500 Gilman Dr, MC 0949, La Jolla, CA 92093-0949. Received June 24, 2011; revision requested August 11; revision received October 13; accepted October 28; final version accepted November 14. **Address correspondence to** J.B.B. (e-mail: *jbrewer@ucsd.edu*).

Parkinson-related dementia (PRD) is the second most common cause of neurodegenerative dementia in the United States, estimated to make up 15%–35% of all patients with dementia (1). Patients with PRD may experience the motor symptoms of parkinsonism, as well as cognitive impairment that is frequently confused with Alzheimer disease (1–3). Subtypes of PRD include Parkinson disease (PD) dementia and dementia with Lewy bodies, but there is substantial overlap in the neuropathologic and cognitive profile of these disorders. Both disorders share a pathologic hallmark in the presence of Lewy bodies, which are filamentous inclusions consisting of the presynaptic protein α-synuclein. Clinically, these disorders are primarily distinguished by the order of symptom onset. However, early detection and differential diagnosis of these disorders can prove challenging, especially when Lewy body disease spreads to cortical brain regions and the clinical profile may resemble Alzheimer disease. Additionally, synuclein and amyloid pathologic conditions often coexist in patients with dementia with Lewy bodies, which further confounds detection and diagnosis of these disorders (1–4).

A noninvasive imaging biomarker is needed to advance basic scientific investigation of Parkinson-related disorders in vivo, as well as to aid in diagnosis and evaluation of treatment effects in clinical research and practice. Interregional correlations of the resting blood oxygen level–dependent functional magnetic resonance (MR) imaging signal constitute one area of active interest in the search for biomarkers. Functional imaging biomarkers are particularly attractive in that they may be able to depict disease prior to widespread atrophy and could reflect therapeutic effects on a shorter time scale than structural techniques. Resting functional MR imaging has a strong clinical appeal because it affords the ability to study multiple networks of the entire brain at once and, relative to task-based functional MR imaging, it is less susceptible to the confounding effects of cognitive ability to perform a given behavioral task (5–9). Variations in resting functional correlations (often termed *functional connectivity*) have already been reported in several neurologic disorders, including Alzheimer disease (10,11), mild cognitive impairment (12–14), and PD (15,16). Changes in Alzheimer disease were shown within regions termed the *default network,* while changes in PD have been described in correlations between the cortex and the striatum. Some early reports have even suggested that resting functional correlations may be sensitive to neurologic changes prior to the onset of clinical symptoms in neurodegenerative disease (17,18). It is unknown whether resting functional MR imaging might be a useful biomarker in PRD.

In the present study we apply a recently developed native-space (or native-surface) method (19) to compare resting functional MR imaging correlations (functional connectivity) measured in patients with PRD to those measured in cognitively unimpaired, age-matched control subjects with or without PD. We hypothesized that PRD would be associated with altered interregional blood oxygen level–dependent correlations both within the default network and between corticostriatal regions.

Advances in Knowledge

- Relative to healthy aging, Parkinson-related dementia (PRD) patients exhibited decreased resting functional MR imaging correlation between a priori selected corticostriatal regions.
- Interregional default-network correlations were similar between PRD patients, patients with Parkinson disease, and healthy elderly individuals.
- Disruption of corticostriatal functional correlations was detected in PRD patients in relative absence of regional structural changes.

Materials and Methods

Participant Characteristics

Participant characteristics are provided in Table 1. A total of 60 recruited participants (20 with PD, 18 with PRD, 22 age-matched control subjects) underwent resting-state imaging for this prospective study between January 2010 and May 2011. Consent was provided by all participants, and the study was approved by an institutional review board and complied with Health Insurance Portability and Accountability Act regulations. General inclusion criteria were men and women between the ages of 55 and 100 years with a diagnosis of being cognitively normal or having PD or PRD. Movement disorder specialists evaluated the participants with PD and PRD and made diagnoses based on established criteria (1,3); participants meeting criteria for dementia with Lewy bodies or PD dementia were included in the PRD group. General exclusion criteria were MR imaging contraindications, history of symptomatic stroke or other major neurologic or psychiatric disorder, and inability to adequately communicate with the operator of the imager. Data from four subjects were excluded from analysis due to poor quality: T1-weighted volume (n = 2), excessive motion during imaging (n = 1), and anterior drop-out (n = 1). Thus, data from 56 participants (19 with PD, 18 with PRD, 19

Published online before print
10.1148/radiol.12111280 **Content code:** NR

Radiology 2012; 263:226–234

Abbreviations:
ANOVA = analysis of variance
PD = Parkinson disease
PRD = Parkinson-related dementia

Author contributions:
Guarantors of integrity of entire study, T.M.S., J.B.B.; study concepts/study design or data acquisition or data analysis/interpretation, all authors; manuscript drafting or manuscript revision for important intellectual content, all authors; approval of final version of submitted manuscript, all authors; literature research, T.M.S., J.B.B.; clinical studies, E.A.M., J.B.B.; experimental studies, T.M.S., J.B.B.; statistical analysis, T.M.S., E.A.M., J.B.B.; and manuscript editing, T.M.S., J.B.B.

Funding:
This research was supported by the National Institutes of Health (grants 5K02NS067427, P50AG005131, and 5 T32 GM007198).

Potential conflicts of interest are listed at the end of this article.

Table 1

Participant Characteristics

Participant Group	Age (y)	Education (y)	MMSE*
Elderly control ($n = 19$)	76 ± 9 (58–90)	17 ± 2 (13–20)	29.0 ± 1.1 (27–30)
Male ($n = 8$)	76 ± 11 (61–90)	18 ± 3 (13–20)	28.5 ± 0.9 (27–30)
Female ($n = 11$)	76 ± 8 (58–83)	17 ± 2 (13–20)	29.5 ± 1.0 (27–30)
PD ($n = 19$)	70 ± 8 (57–84)	17 ± 3 (12–20)	29.0 ± 1.3 (26–30)
Male ($n = 12$)	69 ± 7 (59–80)	17 ± 3 (12–20)	29.2 ± 1.1 (27–30)
Female ($n = 7$)	72 ± 8 (57–84)	17 ± 3 (12–20)	28.6 ± 1.6 (26–30)
PRD ($n = 18$)	72 ± 7 (61–97)	16 ± 2 (12–20)	23.3 ± 4.6 (13–30)
Male ($n = 16$)	74 ± 9 (61–97)	16 ± 2 (12–20)	23.6 ± 4.4 (13–30)
Female ($n = 2$)	68 ± 4 (65–70)	18	16

Note.—Data are means ± standard deviation, with range in parentheses. Years of education were unobtainable for one PRD female participant. Dementia rating score (20) was obtained instead of Mini-Mental State Examination score for two male PD and one female PRD participants; these were at ceiling for the two PD participants, and 130 (impaired) for the PRD participant.

* MMSE = Mini-Mental State Examination (21).

age-matched control subjects) were analyzed.

MR Imaging Acquisition

Structural and functional imaging procedures were described previously (19). Two T2*-weighted sequences of approximately 7 minutes each were performed for each participant with a 1.5-T system (GE Healthcare, Waukesha, Wis) (repetition time msec/echo time msec, 2624/45; flip angle, 90°; matrix, 64 × 64; voxel size, 3.75 × 3.75 × 5 mm; 32 adjacent sagittal sections; 155 samples per series). Immediately prior to each functional series, a spin-echo volume was acquired with opposite phase-encoding polarity for field inhomogeneity (22). Participants were asked to rest motionless with eyes open during the functional sequences (23,24). In addition to the functional volumes, a high-resolution, three-dimensional, T1-weighted volume was acquired for each subject (8.5/3.8; inversion time, 500 msec; flip angle, 10°; matrix, 256 × 256 × 256; voxel size, 0.9375 × 0.9375 × 1.2000 mm). Respiratory effort and heart rate were monitored and recorded with a pressure transducer and a pulse oximeter, respectively (BioPac Systems, Goleta, Calif).

Structural MR Imaging Processing

A model of each subject's cortical surface was reconstructed from the T1-weighted MR imaging volume (25,26). The surface was then anatomically parcellated by using the Desikan-Killiany atlas (27,28). Subcortical structures were similarly identified by means of volume segmentation (29). Results from each of these automated steps were inspected for accuracy, and manual corrections were applied as necessary (E.A.M., with 2 years of experience in editing data from more than 100 examinations and trained by experts in the field) according to the procedures described previously, ensuring accurate native surfaces (19). Regions used in the functional analysis were tested for group differences in cortical thickness (or subcortical volume, after adjusting for intracranial volume) by using analysis of variance (ANOVA).

Interregional Correlation Analysis with Functional MR Imaging

Procedures for functional MR imaging correlation analysis on native surfaces have been described in detail elsewhere (19). Briefly, these procedures take advantage of automated FreeSurfer parcellation tools (Athinoula A. Martinos Center for Biomedical Imaging, Charlestown, Mass) and avoid transformation of functional data to an atlas volume. A single parcellated region from each individual surface or native volume is used as the seed for each hemisphere (a seed is a region of particular interest believed to contribute to a particular function, dysfunction, or network). The functional time series from the seed is then correlated with the average time series from the other regions in the Desikan-Killiany atlas by calculating a Pearson correlation coefficient between the seed time series and each region's average time series. Finally, Fisher z transform is applied to the correlation coefficients. Region time series is obtained by loading the subject's functional data and parcellated native surface by using software (MATLAB 2009b; Mathworks, Natick, Mass); a time series at each vertex is classified by the region code at the corresponding location in the parcellated surface.

Vertex-wise correlation analysis (surface equivalent of voxel-wise analysis) was also performed. Individual maps were produced by calculating the Fisher z-transformed correlation coefficient for the average seed region time series and the time series of each vertex on the surface. Individual native surfaces were registered to the FreeSurfer fsaverage map (19). Group maps were created by loading individual fsaverage maps with MATLAB and computing the mean across subjects. Visualization thresholds were set on the basis of the group map for control subjects; the minimum threshold was 0.5 standard deviation above the mean, and the maximum threshold was 1.5 standard deviations above the mean. To account for possible variation in functional anatomy, individual maps were subjected to surface-based smoothing (approximately equivalent to a 6-mm Gaussian kernel in two dimensions) prior to performance of vertex-wise group statistics. All group summary maps were similarly smoothed for display. Tissue mislabeling can frequently arise during transformation to a volume atlas such as Talairach or MNI152 (Montreal Neurological Institute, Montreal, Quebec, Canada), introducing large effects on functional correlations; surface-based registration reduces these errors (19,26,30).

Analyses were performed with two seed regions. The isthmus cingulate has been shown to be a reliable seed for study of the default network (19). Additionally, the caudate was also chosen as a seed to investigate

Table 2

Native-Surface Correlation Analysis for Default-Network (Isthmus Cingulate Seed) and Corticostriatal Correlations (Caudate Seed)

	Left Hemisphere					Right Hemisphere				
	Control	PD		PRD		Control	PD		PRD	
Region	*r* Value	*r* Value	*P* Value	*r* Value	*P* Value	*r* Value	*r* Value	*P* Value	*r* Value	*P* Value
Isthmus cingulate										
Superior frontal	0.90 (0.07)	0.83 (0.07)	.54	0.70 (0.07)	.06	0.91 (0.06)	0.77 (0.07)	.17	0.71 (0.06)	.03
Inferior parietal	0.94 (0.07)	0.90 (0.07)	.71	0.87 (0.06)	.43	0.90 (0.06)	0.88 (0.06)	.88	0.82 (0.06)	.39
Medial orbitofrontal	0.63 (0.06)	0.62 (0.06)	.86	0.42 (0.06)	.03	0.55 (0.06)	0.53 (0.07)	.87	0.42 (0.06)	.15
Hippocampus	0.65 (0.07)	0.68 (0.09)	.78	0.58 (0.05)	.44	0.63 (0.05)	0.58 (0.06)	.55	0.48 (0.05)	.03
Parahippocampal	0.50 (0.07)	0.62 (0.09)	.27	0.56 (0.06)	.49	0.62 (0.05)	0.51 (0.06)	.16	0.50 (0.05)	.11
Caudate										
Putamen	0.83 (0.06)	0.78 (0.07)	.55	0.63 (0.07)	.03*	0.98 (0.08)	0.83 (0.06)	.14	0.68 (0.07)	.007†
Superior frontal	0.98 (0.05)	0.83 (0.08)	.13	0.69 (0.08)	.006†	0.86 (0.07)	0.70 (0.08)	.16	0.65 (0.06)	.03†
Caudal middle frontal	0.70 (0.06)	0.58 (0.07)	.23	0.47 (0.07)	.02†	0.81 (0.06)	0.61 (0.07)	.04	0.48 (0.07)	.001†
Rostral anterior cingulate	0.46 (0.06)	0.52 (0.07)	.54	0.52 (0.07)	.51	0.28 (0.06)	0.35 (0.06)	.46	0.34 (0.07)	.56
Rostral middle frontal	0.81 (0.06)	0.72 (0.08)	.38	0.66 (0.08)	.14	0.87 (0.05)	0.69 (0.07)	.06	0.57 (0.07)	.001†

Note.—Unless otherwise indicated, data are population mean *z*-transformed correlation coefficients and data in parentheses are standard error. There was no significant difference between PD and PRD patients (*P* values not shown) or between PD patients and control subjects. Regions were selected a priori based on strength of correlation with the respective seed in independent data sets.

* Trend toward significance (false-discovery rate = 0.052; no other values survive false-discovery rate controlled at < 0.10).

† Significant after correction for multiple comparisons.

corticostriatal correlations. Dopaminergic projections to the striatum are affected by PD, and the caudate has been particularly implicated in cognitive functions (31,32). Greater caudate atrophy has been reported in PD dementia patients than in PD patients without dementia (33). Further, in patients with PD, a structural change in the caudate has been shown to correlate with various measures of executive function, including the Stroop Test, the Trail Making Test, and the Digit Ordering Test (34). Each of these regions has been evaluated as a seed in another data set using healthy adults (19,35). To avoid unnecessary multiple comparisons, the five regions most strongly correlated with each seed in that prior data set were selected a priori for regional analyses (Table 2). Vertex-wise analyses were performed for the entire cortical surface.

Statistical Analysis

All statistical analyses were performed by using MATLAB, unless otherwise specified. Subjects with PRD were compared with elderly control subjects with or without PD to test for potential population differences attributable to Parkinson-related disease. Two-sample *t* tests were applied to data from each native-surface region of interest, and results were assessed for significance after controlling the false-discovery rate at less than 0.05 to correct for multiple comparisons (36). Vertex-wise comparisons were also made by using two-sample *t* tests at each vertex on the group surface. Group vertex-wise *t* test maps were smoothed (approximately equivalent to a 12-mm Gaussian kernel in two dimensions) for display. All *t* test results made no assumption of equal variance between groups. Additionally, cortical thickness and basal ganglia were compared for each region across subject groups by using ANOVA after adjusting for age, sex, and intracranial volume (PASW Statistics, GradPack 18; SPSS, Chicago, Ill); significance was assessed after controlling the false-discovery rate at 0.05, as was performed for the functional data. A final ANOVA was performed (PASW Statistics, same threshold for significance) to evaluate whether findings from the functional correlation analyses could be explained by demographic features, including age, sex, and years of education.

Results

Seed regions (caudate and isthmus cingulate) and all regions selected a priori, listed in Table 2, were also tested for a structural effect of disease state. Cortical thickness for surface regions and subcortical volumes (adjusted for intracranial volume) for basal ganglia structures were compared with ANOVA. After controlling the false-discovery rate at 0.05, or 0.10, only the right parahippocampal region was significantly different across groups ($F = 7.905$; $df = 2, 52$; $P = .001$, uncorrected).

Despite the relatively advanced age of the elderly control participants (mean age, >76 years), resting correlation results for this group were generally consistent with previous reports in college-aged and middle-aged adults (19,35). Isthmus cingulate maps (Fig 1, *A*) show characteristic features of the default network, including prominent involvement of medial and inferior lateral parietal areas, as well as medial and lateral prefrontal cortex. Caudate maps differ from isthmus cingulate maps—in particular, the caudate is strongly correlated with areas such as the supplementary motor area, presupplementary motor area,

Figure 1

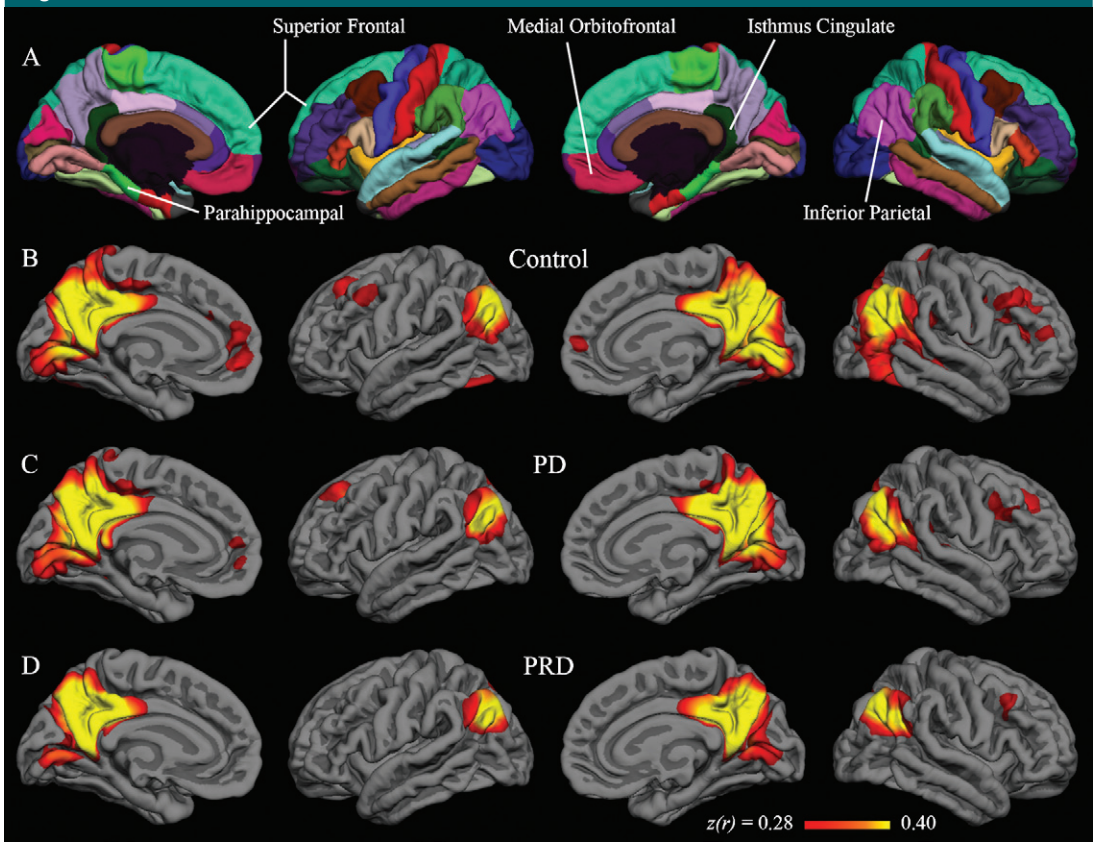

Figure 1: *A,* Desikan-Killiany cortical parcellation atlas. *B–D,* Group correlation maps with isthmus cingulate seed. Fisher *z*-transformed correlation coefficients for the correlation of each vertex on the surface with the average time series of the isthmus cingulate seed. The minimum and maximum thresholds for the functional overlay are 0.5 and 1.5 standard deviations, respectively, above the mean coefficient from the group map for control subjects.

and middle frontal gyrus (Fig 2, *B*), in agreement with known structural connectivity (31,37,38). Table 2 lists the *z*-transformed correlation coefficients for the elderly control group; regions in the table were selected a priori for their strong correlation with the respective seeds in independent data sets. Many of these regions remain strongly correlated with their respective seeds in the present cohort of resting elderly control subjects, further demonstrating the overall qualitative consistency of these data with published resting functional MR imaging data.

To examine for potential effects of PD and PRD on the default network, the strength of resting correlations between default-network regions was compared across groups. Table 2 reports correlation coefficients for default-network regions with the isthmus cingulate seed. Although there are some regions where a pattern of decreased correlation strength is suggested in PRD (especially bilateral superior frontal, left medial orbitofrontal, and right hippocampus), no default region significantly differs between PRD and elderly control subjects or between PD and control subjects, after correcting for multiple comparisons. Indeed, no region showed a significant difference even when the false-discovery rate correction was relaxed only 0.10 (ie, to look for trends). Group maps in Figure 1, *B–D,* also show possibly diminished prefrontal (medial and lateral) involvement with PD and PRD relative to control, but the maps for the three groups are still qualitatively similar. No area of the cortex was significantly different between the groups after correcting for multiple comparisons in vertex-wise tests. For illustration, however, Figure 3, *A,* shows population differences at a very liberal threshold without correction for multiple comparisons ($P < .01$, uncorrected). Although there were some suggestions of small group differences in both region-based and vertex-wise results, in the end there was not a single a priori default-network region or cortical vertex with a significant difference between disease and control groups when the isthmus cingulate was used as a seed.

Corticostriatal resting correlations were also examined for differences

Figure 2

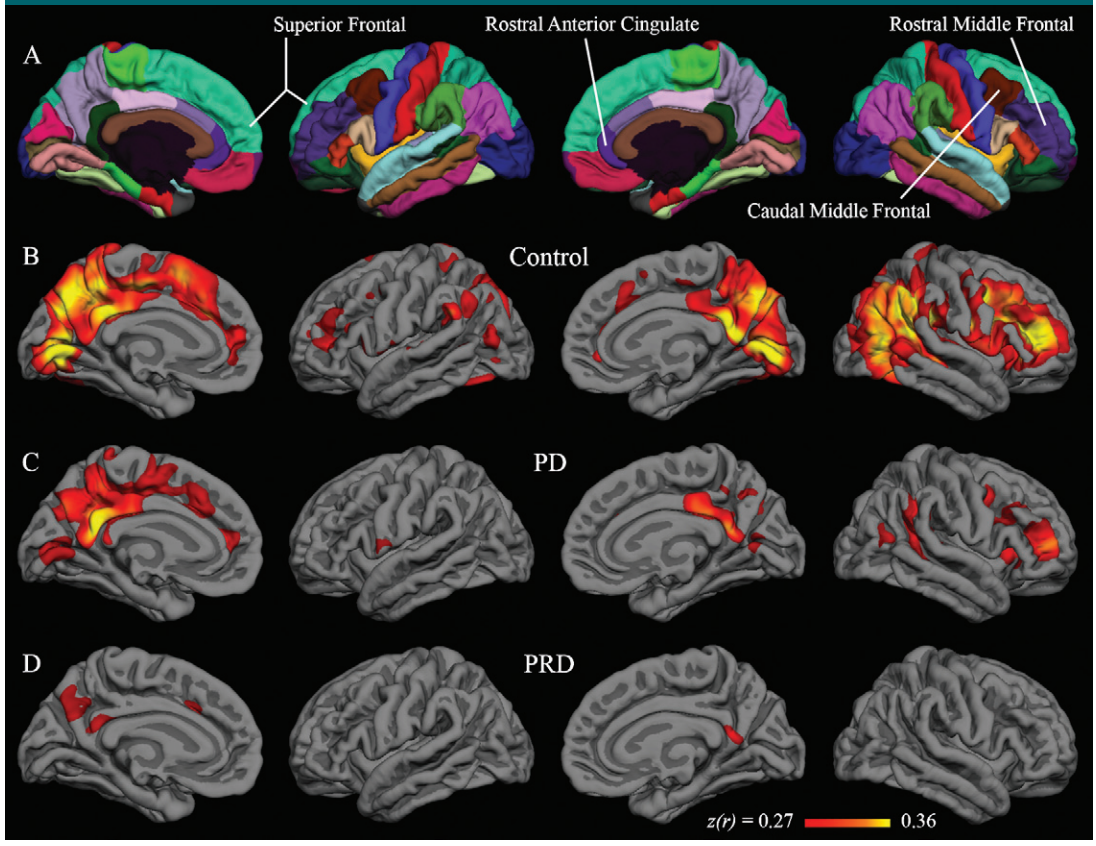

Figure 2: *A,* Desikan-Killiany cortical parcellation atlas. *B–D,* Group correlation maps with caudate seed. Fisher *z*-transformed correlation coefficients for the correlation of each vertex on the surface with the average time series of the caudate seed. The minimum and maximum thresholds for the functional overlay are 0.5 and 1.5 standard deviations, respectively, above the mean coefficient from the group map for control subjects.

across Parkinson-related disease state. Contrary to the isthmus cingulate results, several regions were significantly different in the PRD group relative to the control group Table 2. These included bilateral superior frontal, bilateral caudal middle frontal, and right putamen (left putamen showed a trend toward significance, identified when the false-discovery rate was relaxed to 0.052 instead of 0.05). No a priori region was significantly different in the PD group relative to either the control or PRD group. This pattern is illustrated in Figure 2, where there is a qualitative decrease in both the magnitude and extent of corticostriatal correlations in the PRD maps relative to the control maps, with PD showing an intermediate level of correlations. Figure 3, *B,* further illustrates this qualitative pattern with use of the same threshold as for the default network (Fig 3, *A*). While these vertex-by-vertex differences were not statistically significant in isolated vertices after correction for multiple comparisons (for the entire brain), Figure 3, *B,* shows that the vertex-level contrasts nevertheless highlight the areas where significant region-level differences were found in the corticostriatal network.

An additional ANOVA was performed to determine whether the functional correlation differences described above could be attributed to differences in demographic features. Sex, age, and years of education were included as covariates. None of these covariates had a significant relationship with the strength of functional correlation in any of the regions in Table 2.

Discussion

In the current study, patients with PRD, relative to healthy, age-matched control subjects, exhibited disruption of interregional resting functional MR imaging correlations in corticostriatal networks selected a priori and defined by using subject-specific anatomy. In contrast, similarly defined interregional correlations in the default network were not different for patients with dementia relative to healthy control subjects across most regions. These results suggest that resting networks, identifiable in vivo, may be differentially sensitive to the effects of PRD. Moreover, disruption

Figure 3

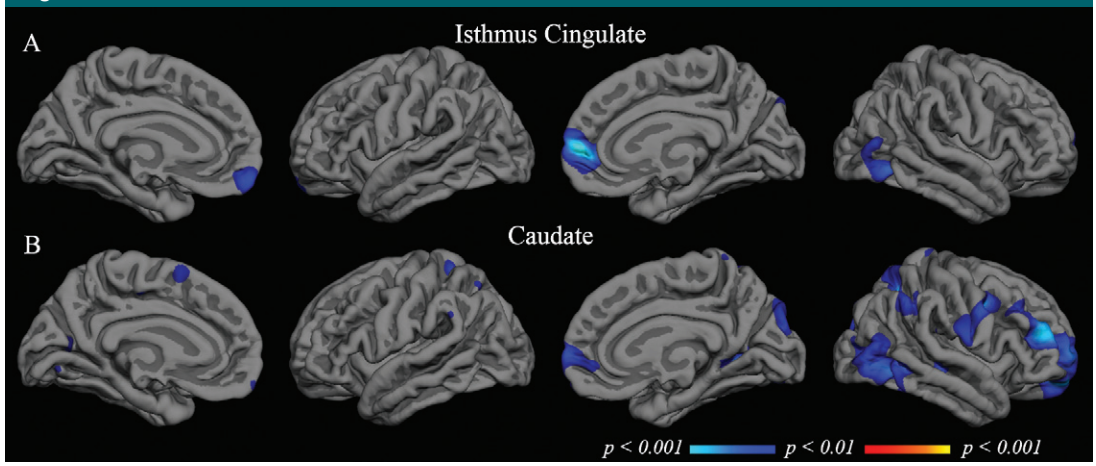

Figure 3: Group *t* test maps. Functional overlays show *t* values for each vertex for the relevant comparison. *A,* Comparison of PRD patients with elderly control subjects when isthmus cingulate is used as the seed (default network). *B,* Comparison of PRD patients with elderly control subjects when the caudate is used as the seed (corticostriatal network). Thresholds set at $P < .01$ (minimum) and $P < .001$ (maximum), without correction for multiple comparisons. "Cool" colors indicate decreased correlation strength in PRD relative to healthy aging, and "warm" colors indicate increased correlation strength in PRD (none found).

of corticostriatal correlations was detected in the absence of statistically significant structural changes in these regions, possibly implying that the functional technique has greater sensitivity to PRD pathologic conditions.

One recent publication (39) reported differences between patients with dementia with Lewy bodies and control subjects in the default network. The suggestion of decreased correlation between a medial parietal seed and prefrontal and medial temporal regions in our own data is consistent with their results, and the differences in both studies were found only when no correction was made for multiple comparisons. Because the Galvin et al (39) study represents the only similar study to our own regarding resting interregional blood oxygen level–dependent correlations in PRD, some consideration of methodological differences between these two studies is important. One primary difference is that Galvin et al compared regions defined functionally by using group contrasts in the same data, whereas we used anatomic regions that were defined a priori from independent data sets acquired in young, healthy adults. Participant selection also differed between the two studies; Galvin et al included only the dementia with Lewy body–subtype of PRD and were able to exclude from their control group (but not the dementia with Lewy bodies) individuals with a high amyloid burden. Similar numbers of PRD participants were included in the two studies (18 in the present study compared with 15 with dementia with Lewy bodies in the previous study), but the Galvin et al study included a larger control group (38 compared with 19 patients). Here we modeled and removed the effects of respiratory fluctuations using the RETROICOR method (40); no method of controlling for physiologic noise was mentioned by Galvin et al. Finally, negative interregional correlations (anticorrelations), present in the results of the Galvin et al study but not in ours, are usually seen only after regression of the mean global signal, a step we did not perform due to concerns about mathematic validity (41) and the associated controversy of interpretation (40–43).

One important challenge for resting functional MR imaging studies in neurodegenerative conditions such as PRD is the potential confound of registration errors in subjects with atrophy. Nearly all available reports of resting interregional functional MR imaging correlations in disease, including all those that have included PD (15,16,44) or PRD (39), have used methods that depend on transformation of functional data to a standard volume (eg, Talairach or MNI152). Even small inaccuracies in the warping of individual brains to the standard volume could result in areas of cerebrospinal fluid or white matter being mistakenly labeled as gray matter. It has recently been shown that such errors can be common, are easily overlooked, and can have large, widespread effects on resting functional MR imaging correlations (19). In the present study we analyzed resting correlations within the native space of individual subjects to avoid such artifacts.

The primary limitation of this study was the inherent diagnostic ambiguity of dementia. Without biopsy, we must rely on imperfect clinical diagnoses to classify the participants (1–3); however, consensus PRD diagnostic criteria used in the present study yield high specificity. A limitation of the present study might be its focus on PRD without inclusion of Alzheimer dementia, which might provide more direct evidence of the technique's potential use for differential diagnosis. However, though Alzheimer disease patients were not included in this study, there have been numerous previous reports of decreased default-network

correlations in subjects with elevated amyloid (10–12,14,17,18,45–50). Finally, a limitation of native-space parcellation analysis is dependence on anatomic regions of interest rather than on functionally defined regions. Functionally defined regions might yield more powerful statistical comparisons between only the most relevant of vertices, but such approaches result in circularity when region selection is identified from the same data set as used for comparison. Anatomically defined regions in native space promote comparison across multiple studies and increase signal-to-noise ratio over single voxels or vertices.

In conclusion, the results of the present study show an association between PRD and disruption of corticostriatal resting functional MR imaging correlations, especially between the caudate and prefrontal cortex. This effect was found by using a simple, noninvasive, resting protocol that could be implemented in existing clinical or research MR imaging systems, and the functional difference was detected despite an absence of significant differences in structural MR imaging. Thus, these results suggest that resting corticostriatal correlations may be a sensitive biomarker for basic investigation of PRD and for clinical evaluation of patients or for therapeutic interventions. Furthermore, it is intriguing that the two existing resting functional MR imaging studies of PRD both show a lack of significant changes in default-network correlations, raising the possibility of selective vulnerability in dementia that depends on underlying etiology. Disease specificity has already been reported for fronto-temporal dementia and Alzheimer disease (51); if true for PRD as well, this technique may have potential diagnostic utility in distinguishing PRD from other dementias when clinical diagnosis is ambiguous.

Acknowledgments: The authors thank collaborators at the UCSD Parkinson's Disease Research Consortium, Shiley-Marcos Alzheimer's Disease Research Center, Multi-modal Imaging Laboratory, Center for Functional MR imaging, Radiology Imaging Laboratories, and clinicians at the UCSD Medical Center. We also express our appreciation to Jerlyn Tolentino for help with recruitment and data acquisition.

Disclosures of Potential Conflicts of Interest: T.M.S. Financial activities related to the present article: as an MSTP student, author received money for tuition/fees and a standard student stipend from NIH while working toward a PhD degree, as well as money for travel expenses for meeting in Wisconsin (International Conference on Resting-State Functional Brain Connectivity). Financial activities not related to the present article: none to disclose. Other relationships: none to disclose. **E.A.M.** No potential conflicts of interest to disclose. **E.J.K.** Financial activities related to the present article: institution received a grant from NIH. Financial activities not related to the present article: none to disclose. Other relationships: none to disclose. **J.B.B.** Financial activities related to the present article: institution received grants (NINDS K02 NS067427, NIA U01 AG10483, NIA P50 AG005131, NIA RC2AG036535, NIA R01AG034062) from NIH and a grant from General Electric Medical Foundation. Financial activities not related to the present article: author is board member of the Elan Pharmaceuticals Imaging Advisory Board, Lilly Biomarkers Business Unit Advisory Board, and Avanir Pharmaceuticals Advisory Board; institution receives research support from Janssen Alzheimer Immunotherapy (Site PI for Bapineuzumab and ACC Trials); and author owns stock options in CorTechs Labs. Other relationships: none to disclose.

References

1. Geser F, Wenning GK, Poewe W, McKeith IG. How to diagnose dementia with Lewy bodies: state of the art. Mov Disord 2005; 20(Suppl 12):S11–S20.
2. Lippa CF, Duda JE, Grossman M, et al. DLB and PDD boundary issues: diagnosis, treatment, molecular pathology, and biomarkers. Neurology 2007;68(11):812–819.
3. McKeith IG. Dementia with Lewy bodies and Parkinson's disease with dementia: where two worlds collide. Pract Neurol 2007;7(6):374–382.
4. Galvin JE, Pollack J, Morris JC. Clinical phenotype of Parkinson disease dementia. Neurology 2006;67(9):1605–1611.
5. Auer DP. Spontaneous low-frequency blood oxygenation level-dependent fluctuations and functional connectivity analysis of the 'resting' brain. Magn Reson Imaging 2008; 26(7):1055–1064.
6. Fox MD, Raichle ME. Spontaneous fluctuations in brain activity observed with functional magnetic resonance imaging. Nat Rev Neurosci 2007;8(9):700–711.
7. Greicius MD. Resting-state functional connectivity in neuropsychiatric disorders. Curr Opin Neurol 2008;21(4):424–430.
8. van den Heuvel MP, Hulshoff Pol HE. Exploring the brain network: a review on resting-state fMRI functional connectivity. Eur Neuropsychopharmacol 2010;20(8): 519–534.
9. Rogers BP, Morgan VL, Newton AT, Gore JC. Assessing functional connectivity in the human brain by fMRI. Magn Reson Imaging 2007;25(10):1347–1357.
10. Greicius MD, Srivastava G, Reiss AL, Menon V. Default-mode network activity distinguishes Alzheimer's disease from healthy aging: evidence from functional MRI. Proc Natl Acad Sci U S A 2004;101(13): 4637–4642.
11. Sorg C, Riedl V, Perneczky R, Kurz A, Wohlschläger AM. Impact of Alzheimer's disease on the functional connectivity of spontaneous brain activity. Curr Alzheimer Res 2009;6(6):541–553.
12. Bai F, Watson DR, Yu H, Shi Y, Yuan Y, Zhang Z. Abnormal resting-state functional connectivity of posterior cingulate cortex in amnestic type mild cognitive impairment. Brain Res 2009;1302:167–174.
13. Pihlajamäki M, Jauhiainen AM, Soininen H. Structural and functional MRI in mild cognitive impairment. Curr Alzheimer Res 2009; 6(2):179–185.
14. Sorg C, Riedl V, Mühlau M, et al. Selective changes of resting-state networks in individuals at risk for Alzheimer's disease. Proc Natl Acad Sci U S A 2007;104(47): 18760–18765.
15. Helmich RC, Derikx LC, Bakker M, Scheeringa R, Bloem BR, Toni I. Spatial remapping of cortico-striatal connectivity in Parkinson's disease. Cereb Cortex 2010;20(5): 1175–1186.
16. Wu T, Wang L, Chen Y, Zhao C, Li K, Chan P. Changes of functional connectivity of the motor network in the resting state in Parkinson's disease. Neurosci Lett 2009;460(1): 6–10.
17. Hedden T, Van Dijk KRA, Becker JA, et al. Disruption of functional connectivity in clinically normal older adults harboring amyloid burden. J Neurosci 2009;29(40): 12686–12694.
18. Sheline YI, Raichle ME, Snyder AZ, et al. Amyloid plaques disrupt resting state default mode network connectivity in cognitively normal elderly. Biol Psychiatry 2010;67(6): 584–587.
19. Seibert TM, Brewer JB. Default network correlations analyzed on native surfaces. J Neurosci Methods 2011;198(2):301–311.

20. Jurica PJ, Leitten CL, Mattis S. DRS-2: Dementia rating scale-2: professional manual. Lutz, Fla: Psychological Assessment Resources, 2001.

21. Folstein MF, Folstein SE, McHugh PR. "Mini-mental state:" a practical method for grading the cognitive state of patients for the clinician. J Psychiatr Res 1975;12(3):189–198.

22. Holland D, Kuperman JM, Dale AM. Efficient correction of inhomogeneous static magnetic field-induced distortion in Echo Planar Imaging. Neuroimage 2010;50(1):175–183.

23. Van Dijk KR, Hedden T, Venkataraman A, Evans KC, Lazar SW, Buckner RL. Intrinsic functional connectivity as a tool for human connectomics: theory, properties, and optimization. J Neurophysiol 2009;103(1): 297–321.

24. Yan C, Liu D, He Y, et al. Spontaneous brain activity in the default mode network is sensitive to different resting-state conditions with limited cognitive load. PLoS ONE 2009;4(5):e5743.

25. Dale AM, Fischl B, Sereno MI. Cortical surface-based analysis. I. Segmentation and surface reconstruction. Neuroimage 1999;9(2):179–194.

26. Fischl B, Sereno MI, Dale AM. Cortical surface-based analysis. II. Inflation, flattening, and a surface-based coordinate system. Neuroimage 1999;9(2):195–207.

27. Desikan RS, Ségonne F, Fischl B, et al. An automated labeling system for subdividing the human cerebral cortex on MRI scans into gyral based regions of interest. Neuroimage 2006;31(3):968–980.

28. Fischl B, van der Kouwe A, Destrieux C, et al. Automatically parcellating the human cerebral cortex. Cereb Cortex 2004;14(1): 11–22.

29. Fischl B, Salat DH, Busa E, et al. Whole brain segmentation: automated labeling of neuroanatomical structures in the human brain. Neuron 2002;33(3):341–355.

30. Fischl B, Sereno MI, Tootell RB, Dale AM. High-resolution intersubject averaging and a coordinate system for the cortical surface. Hum Brain Mapp 1999;8(4): 272–284.

31. Alexander GE, DeLong MR, Strick PL. Parallel organization of functionally segregated circuits linking basal ganglia and cortex. Annu Rev Neurosci 1986;9:357–381.

32. DeLong MR, Georgopoulos AP. Motor functions of the basal ganglia. Compr Physiol 2011;1017–1061.

33. Almeida OP, Burton EJ, McKeith I, Gholkar A, Burn D, O'Brien JT. MRI study of caudate nucleus volume in Parkinson's disease with and without dementia with Lewy bodies and Alzheimer's disease. Dement Geriatr Cogn Disord 2003;16(2):57–63.

34. Camicioli R, Gee M, Bouchard TP, et al. Voxel-based morphometry reveals extranigral atrophy patterns associated with dopamine refractory cognitive and motor impairment in parkinsonism. Parkinsonism Relat Disord 2009;15(3):187–195.

35. Seibert T, Majid DSA, Aron AR, Corey-Bloom J, Brewer JB. Stability of resting fMRI interregional correlations analyzed in subject-native space: a one-year longitudinal study in healthy adults and premanifest Huntington's disease. NeuroImage 2011 Sep 10. [Epub ahead of print]

36. Genovese CR, Lazar NA, Nichols T. Thresholding of statistical maps in functional neuroimaging using the false discovery rate. Neuroimage 2002;15(4):870–878.

37. Lawrence AD, Sahakian BJ, Robbins TW. Cognitive functions and corticostriatal circuits: insights from Huntington's disease. Trends Cogn Sci 1998;2(10):379–388.

38. Leh SE, Ptito A, Chakravarty MM, Strafella AP. Fronto-striatal connections in the human brain: a probabilistic diffusion tractography study. Neurosci Lett 2007;419(2):113–118.

39. Galvin JE, Price JL, Yan Z, Morris JC, Sheline YI. Resting bold fMRI differentiates dementia with Lewy bodies vs Alzheimer disease. Neurology 2011;76(21): 1797–1803.

40. Glover GH, Li TQ, Ress D. Image-based method for retrospective correction of physiological motion effects in fMRI: RETROICOR. Magn Reson Med 2000;44(1): 162–167.

41. Murphy K, Birn RM, Handwerker DA, Jones TB, Bandettini PA. The impact of global signal regression on resting state correlations: are anti-correlated networks introduced? Neuroimage 2009;44(3):893–905.

42. Chang C, Glover GH. Effects of model-based physiological noise correction on default mode network anti-correlations and correlations. Neuroimage 2009;47(4): 1448–1459.

43. Fox MD, Zhang D, Snyder AZ, Raichle ME. The global signal and observed anticorrelated resting state brain networks. J Neurophysiol 2009;101(6):3270–3283.

44. Helmich RC, Janssen MJR, Oyen WJG, Bloem BR, Toni I. Pallidal dysfunction drives a cerebellothalamic circuit into Parkinson tremor. Ann Neurol 2011;69(2): 269–281.

45. Buckner RL, Sepulcre J, Talukdar T, et al. Cortical hubs revealed by intrinsic functional connectivity: mapping, assessment of stability, and relation to Alzheimer's disease. J Neurosci 2009;29(6):1860–1873.

46. Chen G, Ward BD, Xie C, et al. Classification of Alzheimer disease, mild cognitive impairment, and normal cognitive status with large-scale network analysis based on resting-state functional MR imaging. Radiology 2011;259(1):213–221.

47. Koch W, Teipel S, Mueller S, et al. Diagnostic power of default mode network resting state fMRI in the detection of Alzheimer's disease. Neurobiol Aging 2010 Jun 10. [Epub ahead of print]

48. Rombouts S, Scheltens P. Functional connectivity in elderly controls and AD patients using resting state fMRI: a pilot study. Curr Alzheimer Res 2005;2(2):115–116.

49. Sperling RA, Laviolette PS, O'Keefe K, et al. Amyloid deposition is associated with impaired default network function in older persons without dementia. Neuron 2009;63(2):178–188.

50. Supekar K, Menon V, Rubin D, Musen M, Greicius MD. Network analysis of intrinsic functional brain connectivity in Alzheimer's disease. PLOS Comput Biol 2008;4(6):e1000100.

51. Seeley WW, Crawford RK, Zhou J, Miller BL, Greicius MD. Neurodegenerative diseases target large-scale human brain networks. Neuron 2009;62(1):42–52.